Influence of rough surfaces on electrolytic conduction in porous media

Lawrence M. Schwartz, Pabitra N. Sen, and David Linton Johnson
Schlumberger-Doll Research, Old Quarry Road, Ridgefield, Connecticut 06877-4108
(Received 9 March 1989)

There are many examples of porous media in which electrical transport is associated with a pore fluid of conductivity σ_f and a constant excess surface conductivity Σ_s. In all such systems the relation between the effective conductivity $\sigma_{\rm eff}$ and σ_f is nonlinear due to intrinsic geometrical effects. By calculating $\sigma_{\rm eff}$ for a sequence of geometrical models, we show that the character of this relation depends on the degree of surface roughness. In particular, we consider (1) a three-dimensional consolidated sphere pack with a smooth pore-grain interface, (2) a two-dimensional model in which a self-affine fractal interface is generated by a random-walk algorithm, and (3) a two-dimensional model with a fractal Koch-curve interface. For each of these models, the behavior of $\sigma_{\rm eff}$ is shown to be reasonably well described by a simple Padé approximant based on four independently measurable geometrical parameters. Our analysis provides a physical explanation for the puzzling fact that often only a fraction of the total surface charge (as determined by chemical titration) contributes to electrolytic conduction.

I. INTRODUCTION

Two problems of current interest are electrical transport in charged systems[1-3] and the fractal structure of disordered materials.[4-6] In sandstones containing clay minerals (shaly sands) these effects are both present.[7-10] Here the clay particles are charged, and the counter ions required to guarantee electrical neutrality form within a thin double layer which can contribute substantially to the conductivity. Typically, these clay particles are found at the pore-grain interface whose structure is known to be fractal based on neutron scattering and image analysis studies.[5,6] As expected, the strength of the interfacial conductivity is proportional to the charge concentration Q_v. In shaly sands, however, one commonly finds that only a fraction of the clay counter ions contributes to the total conductivity.[8,9] From a practical point of view this behavior is of interest because the excess conduction due to the clay counter ions must be treated separately when electrical measurements are used to estimate a reservoir's hydrocarbon reserves.[7]

In the present paper we argue that the qualitative trends in the electrical behavior of shaly sands can be understood if the effects of interfacial charge and fractal structure are treated on an equal footing. Calculations based on models with a fractal structure show that the local strength of the electric field in the vicinity of the clay particles can be substantially reduced by the roughness of the interface. Counter ions in these low-field regions do not contribute effectively to the conductivity and are thus not easily seen by electrical measurements. In contrast, in porous media with smooth interfaces, the variation in electric field strength is not sufficient to mask the effects of counter-ion conductivity. In order to focus our attention on these geometrical effects we consider models in which the surface conductivity (due to interfacial charge) is salinity *independent*. However, we also suggest a way to deduce the possible salinity dependence of the interfacial conductivity in real porous media using a Padé-approximant scheme.

In Sec. II we review the relevant aspects of the theory and we describe the Padé-approximant scheme. The actual calculations for the three different models are reported in Sec. III. The conclusions of this paper are summarized in Sec. IV.

II. ELECTROLYTIC CONDUCTION

Let us review, briefly, the equations used to describe electrolytic conduction in charged porous media. A central result is that the dc conductivity can be written as a superposition of the solutions of two electrostatics problems, each of which involves a modified surface conductivity which is constant over the pore-grain interface.[3] In systems where the local conductivity $\sigma(\mathbf{r})$ varies in the vicinity of the interface, a useful parameter is

$$\Sigma_s = \int_0^\infty [\sigma(\epsilon)-\sigma_f]d\epsilon \ , \tag{1}$$

where σ_f is the asymptotic conductivity of the bulk pore fluid and ϵ measures the distance along a normal directed into the pore space from the grain boundary. As indicated schematically in Fig. 1, the integrand in Eq. (1) vanishes for values of ϵ much greater than a Debye screening length which is, at most, of order 100 Å. For the purposes of illustrative numerical calculations, of the kind described in Sec. III, a convenient assumption is

$$\Sigma_s = 1 \ , \tag{2}$$

where we have simply assigned a unit excess area to the shaded region shown in Fig. 1. The effective conductivity of such a system can then be written as

$$g(\sigma_f,\Sigma_s)\equiv\sigma_f\tilde{g}(\Sigma_s/\sigma_f) \ ,$$

where $\tilde{g}$ is determined from the solution of the Laplace equation. The conductivity $\sigma_{\rm eff}$ for a system in which we have electrolytic conduction due to cations as well as

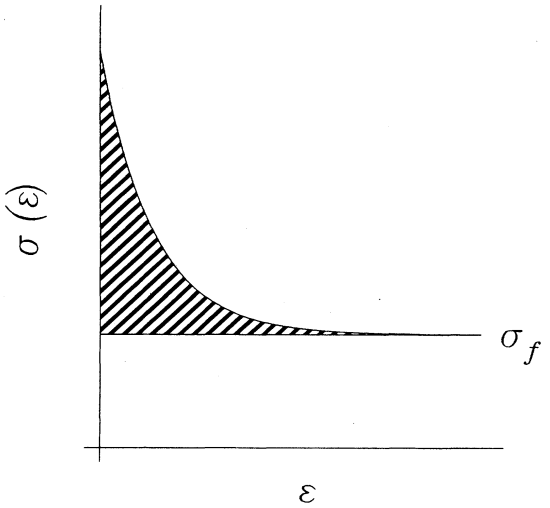

FIG. 1. Schematic representation of the effective conductivity as a function of the distance, ϵ, normal to the grain boundary.

anions is then[3]

$$\sigma_{\text{eff}}=g(\alpha\sigma_f,\beta\Sigma_s)+g((1-\alpha)\sigma_f,(1-\beta)\Sigma_s)\ . \tag{3}$$

Here α and β are the fractions of bulk and surface conduction, respectively, for the cations, and $1-\alpha$ and $1-\beta$ are the corresponding fractions for the anions. We specialize, henceforth, to the case $\alpha=\frac{1}{2}$, $\beta=1$ corresponding to the usual case of comparable cation and anion contributions to bulk conduction and cation dominated surface conduction. To relate Σ_s to the excess charge per unit pore volume, Q_v, we note that Σ_s is the product of the charge per unit area, $Q_v V_p/S$, and the mobility, μ_{DL}, of the counter ions within the double layer

$$Q_v=(S/V_p)(\Sigma_s/\mu_{\text{DL}})\ . \tag{4}$$

(Here V_p/S denotes the pore-volume to surface-area ratio.)

The relation between σ_{eff} and σ_f is, in general, nonlinear. The conventional explanation for the nonlinear character of σ_{eff} considered as a function of σ_f is that the counter-ion mobility increases as a function of salinity.[7] Physically, of course, one would expect the opposite: The mobility should decrease with increasing salinity as the Debye screening length is reduced and the cations become more densely packed. In the present article we explore the consequences of varying degrees of surface roughness on the degree of nonlinearity. First, it will be useful to examine the form of the asymptotic behavior at high and low salinities.

In the limit $\sigma_f\to\infty$ we employ the expansion[10]

$$\lim_{x\to 0}[\tilde{g}(x)]=F^{-1}[1+2x/\Lambda+O((x/\Lambda)^2)]\ , \tag{5a}$$

together with Eq. (3), to get

$$\lim_{\sigma_f\to\infty}\sigma_{\text{eff}}=\frac{1}{F}\left[\sigma_f+\frac{2\Sigma_s}{\Lambda}\right]=\frac{1}{F}[\sigma_f+AQ_v]\ , \tag{5b}$$

where

$$A\equiv(2\mu_{\text{DL}}V_p)/(S\Lambda)\ . \tag{6}$$

Here F and Λ are defined in terms of the solution in the *absence* of any interfacial perturbation.[10] If a uniform external electric field, $\mathbf{E}_{\text{appl}}$ is applied across a cube with side L of an arbitrary porous medium, then

$$F\equiv[\tilde{g}(0)]^{-1}=\frac{L^3|\mathbf{E}_{\text{appl}}|^2}{\int|\mathbf{E}_0(\mathbf{r})|^2\,dV_p} \tag{7a}$$

is the electrical formation factor and

$$\frac{2}{\Lambda}=\frac{\int|\mathbf{E}_0(\mathbf{r})|^2\,dS}{\int|\mathbf{E}_0(\mathbf{r})|^2\,dV_p}\ , \tag{7b}$$

where $\mathbf{E}_0$ is the electric field in the $\Sigma_s\to 0$ limit and the integral in the numerator runs over the pore-grain interface. Note that Λ can be viewed as a *dynamically weighted* version of the length parameter V_p/S. [Indeed, if we ignore the electric field $\mathbf{E}_0(\mathbf{r})$ in Eq. (7b), then $\Lambda\to 2V_p/S$.] Two points should be kept in mind regarding Eq. (5b). First, its intercept, $-AQ_v$, on the negative σ_f axis is proportional to Q_v, and second, the quantity A depends on the *geometry* of the pore space. Standard empirical equations for electrolytic conduction in porous media are of the same form as (5b) but with $A\to\mu_{\text{DL}}$ for all rocks independent of their microgeometry.[7] Within this empirical framework the negative σ_f intercept is taken as a direct measure of Q_v. We will see, however, that the dependence of A on the structure of the interface plays a central role in understanding electrolytic conduction in porous media. We emphasize that (5b) holds true even for a salinity dependent surface conductivity, $\Sigma_s(\sigma_f)$, although our calculations are done for a constant Σ_s.

Consider next the low-salinity limit $\sigma_f\to 0$. Here the expansion[11]

$$\lim_{x\to\infty}[\tilde{g}(x)]=f^{-1}[x+\lambda/2+O(x^{-1})]\ , \tag{8a}$$

together with Eq. (3), allows us to write

$$\lim_{\sigma_f\to 0}\sigma_{\text{eff}}=\frac{1}{f}\left[\Sigma_s+\frac{1}{2}\left[\frac{\lambda}{2}+\frac{f}{F}\right]\sigma_f\right]\ , \tag{8b}$$

where f and λ are defined by analogy with F and Λ:[11]

$$f\equiv\frac{L^3|E_{\text{appl}}|^2}{\int|\mathbf{e}_0(\mathbf{r})|^2\,dS}\ , \tag{9a}$$

is the surface formation factor associated with the excess conductivity Σ_s and

$$\frac{2}{\lambda}\equiv\frac{\int|\mathbf{e}_0(\mathbf{r})|^2\,dS}{\int|\mathbf{e}_0(\mathbf{r})|^2\,dV_p}\ . \tag{9b}$$

[Here $\mathbf{e}_0(\mathbf{r})$ is the electric field in the limit $\sigma_f\to 0$.] Note that both f and λ have the dimensions of length.

For several obvious reasons it is desirable to have a simple but accurate closed-form expression for the conductivity [i.e., for $\tilde{g}(x)$] which is valid over the entire range of conductivity contrast, $x=\Sigma_s/\sigma_f$. Because of their rapidly converging nature, Padé approximants (a ratio of two polynomials) are employed in a wide variety of

such applications.[12] For the problem at hand we wish to construct such a rational function,

$$\tilde{g}_P(x)=\sum_n a_n x^n / \sum_n b_n x^n ,$$

which is exact in the small-x and large-x limits, (5a) and (8a), and accurately reproduces our numerical calculations for arbitrary x. Because of the large-x behavior [Eq. (8a)] the order of the numerator in $\tilde{g}_P$ must be exactly 1 larger than that of the denominator. Because the small-x behavior [Eq. (5a)] is different from that of the large x, the denominator cannot be a constant; it must vary at least linearly. Therefore, the simplest Padé approximant consistent with Eqs. (5a) and (8a) is

$$\tilde{g}_P=\frac{b+cx+dx^2}{1+ax} , \tag{10}$$

where, without loss of generality, the constant in the denominator has been taken equal to be unity. It is straightforward to expand (10) in the limits of small and large x and equate the results with (5a) and (8a), respectively, in order to determine the coefficients a, b, c, and d:

$$a=\frac{2/F\Lambda-1/f}{\lambda/2f-1/F} , \tag{11a}$$

$$b=1/F , \tag{11b}$$

$$c=\frac{1-\lambda/\Lambda}{f-\lambda F/2} , \tag{11c}$$

$$d=\frac{2/F\Lambda-1/f}{\lambda/2-f/F} . \tag{11d}$$

Thus, $\tilde{g}_P$ is constructed in terms of four parameters (f,λ,F, and Λ) which result from the microscopic solution of only two different conductivity problems ($\sigma_f\equiv 0$ and $\Sigma_s\equiv 0$) and it is exact to the leading 2 orders for high and for low salinities. It shall prove interesting to compare Eqs. (10) and (11) against our numerically exact calculations over the intermediate range of conductivity contrasts. We remind the reader that $\tilde{g}_P$ is used for both cation and anion conductivities, as in Eq. (3).

It should be noted that, in a recent paper by Sen, Goode, and Sibbit,[13] an interpolation scheme very similar to our Eq. (10) has been used to fit experimental data on brine saturated reservoir sandstones. Sen *et al.* take the measureable quantity Q_v/σ_f as their independent variable instead of Σ_s/σ_f as we have done, but otherwise their approach is the same as ours. Of course, one of the main points of the present paper is that Σ_s and Q_v are very different variables. We also note that an equation of the form (10) was suggested on physical grounds by Wyllie and Southwick[14] in one of the earliest papers on the interpretation of electrical measurements on shaly sands. We have now given a precise microscopic definition of the geometrical parameters used in the phenomenological approach to the shaly-sand interpretation.

III. GEOMETRICAL MODELS

A. Conductivity calculations

We have solved for σ_{eff} in a sequence of three models of granular porous media. The first set of calculations is based on a periodic version of the grain-consolidation (GC) model.[15] Here one begins with a close-packed simple-cubic array of insulating spheres and then allows the porosity to decrease by uniform growth of the insulating phase into the pore space. The GC model has an essentially smooth pore-grain interface and, in the absence of enhanced surface conduction, the flow of electrical current proceeds from relatively large open pores through narrow throats. (In fact, this pore-throat-pore sequence is characteristic of many granular systems.) Once a given level of consolidation is achieved, the GC model can easily be generalized to include a thin grain-coating layer with constant excess conductivity. We note that, because the GC pore geometry is fairly simple, the difference between the surface and bulk conduction paths is marginal. Indeed, for the GC model we have[10]

$$\frac{2}{\Lambda}=-\frac{S}{V_p}\frac{d\ln\{F\}}{d\ln\{\phi\}}\equiv m(\phi)\frac{S}{V_p} , \tag{12}$$

and, in the porosity range $0.15\le\phi\le 0.40$, $m(\phi)$ is essentially constant[3,15] with the value 1.60. Since Λ is then proportional to V_p/S, the parameter A [recall (5)] is *the same* for all porosities in this range and the negative σ_f intercept is expected to be proportional to Q_v. The results presented in Fig. 2 and Table I show that this is, in fact, the case. Note, further, that the Padé approximant (dashed curve) provides an excellent description of the salinity dependence of σ_{eff} in the intermediate salinity regime. On the scale of Fig. 2 it appears that $\sigma_{\text{eff}}(\sigma_f)$ is nearly linear but this is not so; the actual conductivity for low values of σ_f is about a factor of 2 less than that implied by 5(a) and 5(b).

Consider next a two-dimensional model in which the pore-grain interface is a self-affine fractal curve generated by a random walk (Fig. 3).[16] Note that the flow of current can again be viewed as a pore-throat-pore series path. It will be instructive to study the electrical conductivity of this model as a function of the surface roughness. One way of doing this is to simply average over successively larger intervals. Thus, we began with a model based on 243 horizontal bonds and then averaged over

TABLE I. Results for GC model at two porosities. Here the width of the enhanced conductivity layer is $\delta R=0.03$.

Grain radius	ϕ	f	λ	F	Λ	$2V_p/S$
1.10	0.3281	1.7507	1.5456	5.3084	0.3799	0.4749
1.25	0.1488	2.7612	0.5445	17.2066	0.2303	0.3040

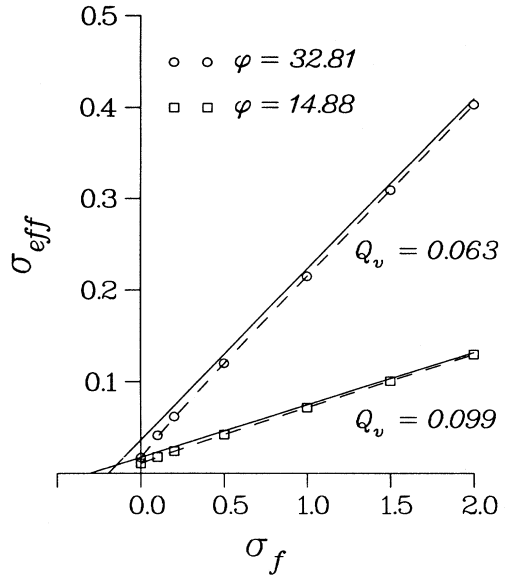

FIG. 2. Effective conductivities for the simple-cubic GC model at two porosities. (The radii of the overlapping spherical grains are $R = 1.10$ and 1.25, respectively, and the thickness of the grain-coating layer is taken equal to 0.03.) The solid lines are the high-salinity asymptotes and the dashed lines are the corresponding Padé approximants.

intervals of length 3, 9, 27, and 81 (Fig. 4). (Factors of 3^n were used to generate a family of interfaces that are, in some sense, analogous to the triadic Koch curves to be discussed next.) Note that, as the level of roughness increases, the two-dimensional analog of S/V_P (and hence Q_v) diverges. In Fig. 5 results are compared for interfaces with three and 243 independent horizontal steps. Here, as in Fig. 2, the system with the lower formation factor and the higher value of Q_v has the high-salinity asymptote with the larger negative σ_f intercept. The results of these two calculations are summarized in Table II. In both cases the σ_{eff} versus σ_f relation is nonlinear

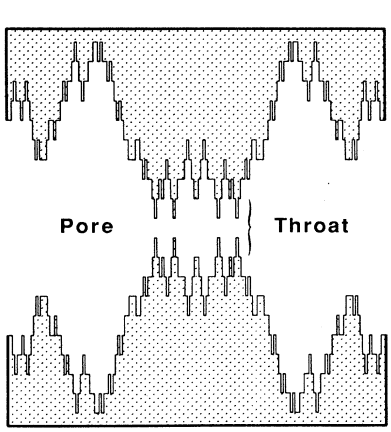

FIG. 3. Two-dimensional pore space with self-affine fractal interface. We are concerned with the flow of electrical current from left to right.

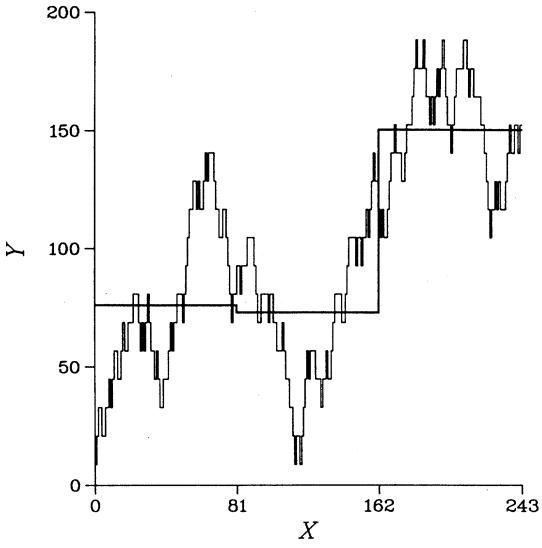

FIG. 4. In the lower left-hand quadrant of a pore space similar to that shown in Fig. 3, we show the original self-affine interface (generated by unit horizontal steps) (thin curve) and the result of averaging this curve over intervals of length 81.

but is well described by (5b) and (8b) in the high- and low-salinity limits, respectively, and by the Padé approximant throughout. Clearly, increased surface roughness implies increased departure from linearity. We note, however, from the values of the geometrical parameters given in Table II, that the ratio of these intercepts seriously underestimates the ratio of the corresponding Q_v values. In other words, while going from the coarse to the fine grid, the value of Q_v has changed by a factor of 6.53, the value of Λ has changed by only a factor of 2.79.

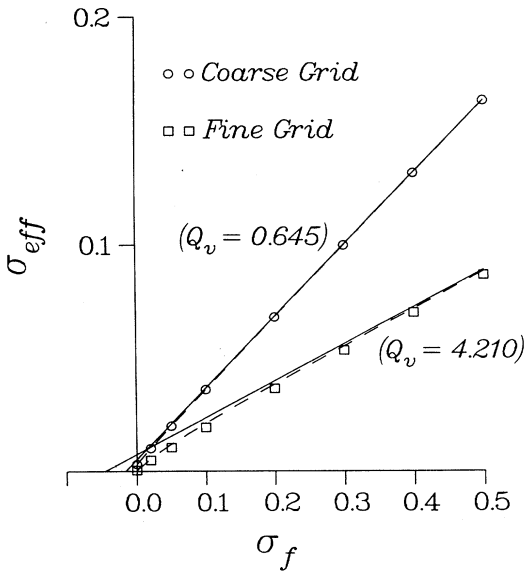

FIG. 5. Effective conductivities for the two-model pore spaces based on the self-affine curves shown in Fig. 4. The solid lines are the high-salinity asymptotes and the dashed lines are the corresponding Padé approximants.

TABLE II. Results for coarse and fine grid self-affine fractal calculations. The number of horizontal steps in the interface is given by 3^n where n is the roughness level number.

Roughness level	ϕ	f	λ	F	Λ	$2V_p/S$
1	0.513	324	285.0	3.157	122.55	310.26
5	0.520	2140.0	1834.0	6.129	43.98	47.50

Physically, this reflects the fact that Λ is more closely related to the effective throat size and is not necessarily controlled by the amount of surface area.

In the third model (Fig. 6) we have a two-dimensional system with a fractal interface generated by the triadic–Koch-curve algorithm. Here, again, the flow of current proceeds from large open pores through narrow throats and back into the larger pores. Superimposed on this basic structure we have added successive levels of interfacial roughness; in Fig. 6 the third-generation interface ["Koch$^{(3)}$"] is shown. Here, again, the value of Q_v diverges as the degree of roughness increases. In Fig. 7 the effective conductivity as a function of σ_f is shown for the extremes of surface roughness we have considered. The results of these two calculations are summarized in Table III. Here, as in Fig. 5, increased surface roughness leads to an increased departure from linearity but once again the Padé approximant follows the numerical calculations rather well.

Of great interest in Fig. 7 is the fact that the fifth-generation (Koch$^{(5)}$) model has a noticeably *smaller* negative intercept, $-AQ_v$, than does the first-generation (Koch$^{(1)}$) model even though the former system has the greater value of Q_v by a factor of roughly 3.67. This is precisely the kind of anomaly that is often seen in shaly sands.[8,9] The key to understanding this behavior is in the variation of the Λ parameter. From Eq. (7b) it is clear that Λ is simply the ratio of the volume and surface averages of the Joule heating loss $|\mathbf{E}_0|^2\sigma$. A display of these losses is shown in Fig. 8. Clearly, the local electric field is greatly reduced over much of the fractal interface. Thus, while we might naively expect [from (7b)] that $\Lambda \to 0$ as $S/V_p \to \infty$, it turns out that Λ *increases* slightly in going from the Koch$^{(1)}$ to the Koch$^{(5)}$ system (Table III). Physically, the essential point is that in this model, the size of the throat does not significantly change as the interface is roughened. In this connection, we note that the dc flow of a viscous fluid is expected to be roughly the same for these two systems. Indeed, since the fluid velocity vanishes at the pore-grain interface, the permeability k should be even less sensitive to surface roughness than the formation factor, F. In Ref. 10 it was suggested that the relation

$$k \approx \Lambda^2/(4F) \tag{13}$$

could be used to estimate the permeability of a porous medium. Interestingly, the results in Table III show that this estimate predicts essentially the same value of k for Koch$^{(1)}$ and Koch$^{(5)}$ systems. While this is in accord with our intuition we note that the conventional permeability estimate, $k \approx (V_p/S)^2/F$, predicts a decrease in k by more than a factor of 10. It is gratifying to see this additional evidence that the Λ parameter provides the relevant length scale for describing transport processes in porous media.

To better understand the relation between the results

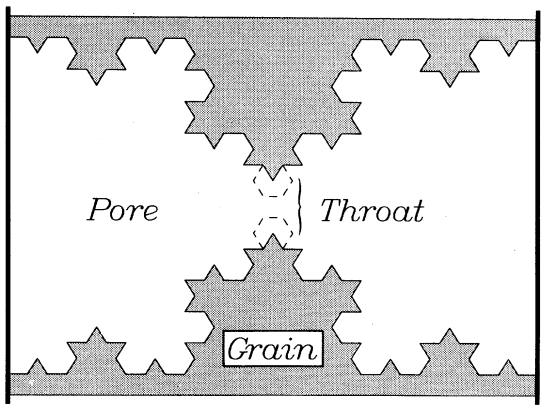

FIG. 6. Two-dimensional Koch triadic–curve model illustrated at the third level of surface roughness. When the grain shape is modified to fill the region outlined by the dashed lines, there is a dramatic change in the electrical conduction (see Fig. 9).

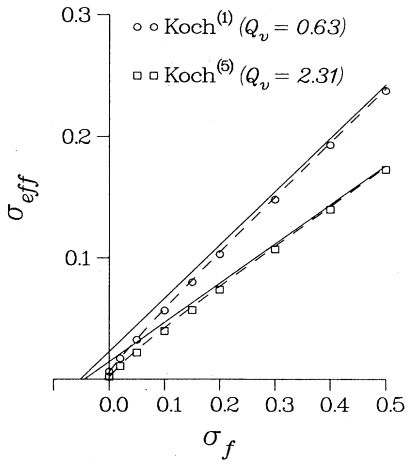

FIG. 7. Effective conductivities for the first and fifth levels of interfacial roughness in the triadic–Koch-curve models. The solid and dashed lines are, respectively, the high-salinity asymptote and the Padé approximant.

TABLE III. Results for Koch[1] and Koch[5] calculations.

Roughness level	ϕ	f	λ	F	Λ	$2V_p/S$
1	0.736	162.0	240.70	2.48	38.53	319.0
5	0.633	512.0	815.00	3.08	44.77	86.8

presented in Figs. 5 and 7, let us consider the modification of the Koch[3] interface depicted in Fig. 6. Here, without changing the length scale on which the interface varies, we have introduced a modification representing growth of the grain into the crucial throat region. This has the effect of placing additional interfacial charge in precisely the region where the electric field is the strongest [see Fig. (8)], as opposed, for example, to the situation when we simply change from a Koch[3] to a Koch[4] interface. As we see in Fig. 9, this modification has a drastic effect on the intercept value (Λ decreases from 38.31 to 20.63) despite the fact that Q_v has increased by less than 5%. Thus the behavior of the intercept AQ_v is again seen to be controlled by the *spatial configuration* of the conducting surface charge rather than simply by its *amount.* Referring back to Fig. 4 for the self-affine fractal surface we see that increased roughness is accompanied by a narrowing of the throat, which implies a reduction in the value of Λ, and, therefore, a predicted increase in the value of the negative intercept AQ_v; precisely this behavior is seen in Fig. 5.

B. Validity of the Padé approximant

Here we wish to consider two closely related issues: the accuracy of the Padé-approximant scheme and its usefulness in determining any salinity dependence to Σ_s from experimental data. The accuracy of the scheme as indicated in Figs. 2, 5, and 7 is slightly misleading because these figures cover only a limited range of salinities, and so we wish to explore this issue further. Secondly, we imagine a hypothetical porous medium for which $\sigma_{\text{eff}}(\sigma_f)$ has been measured and for which the parameters

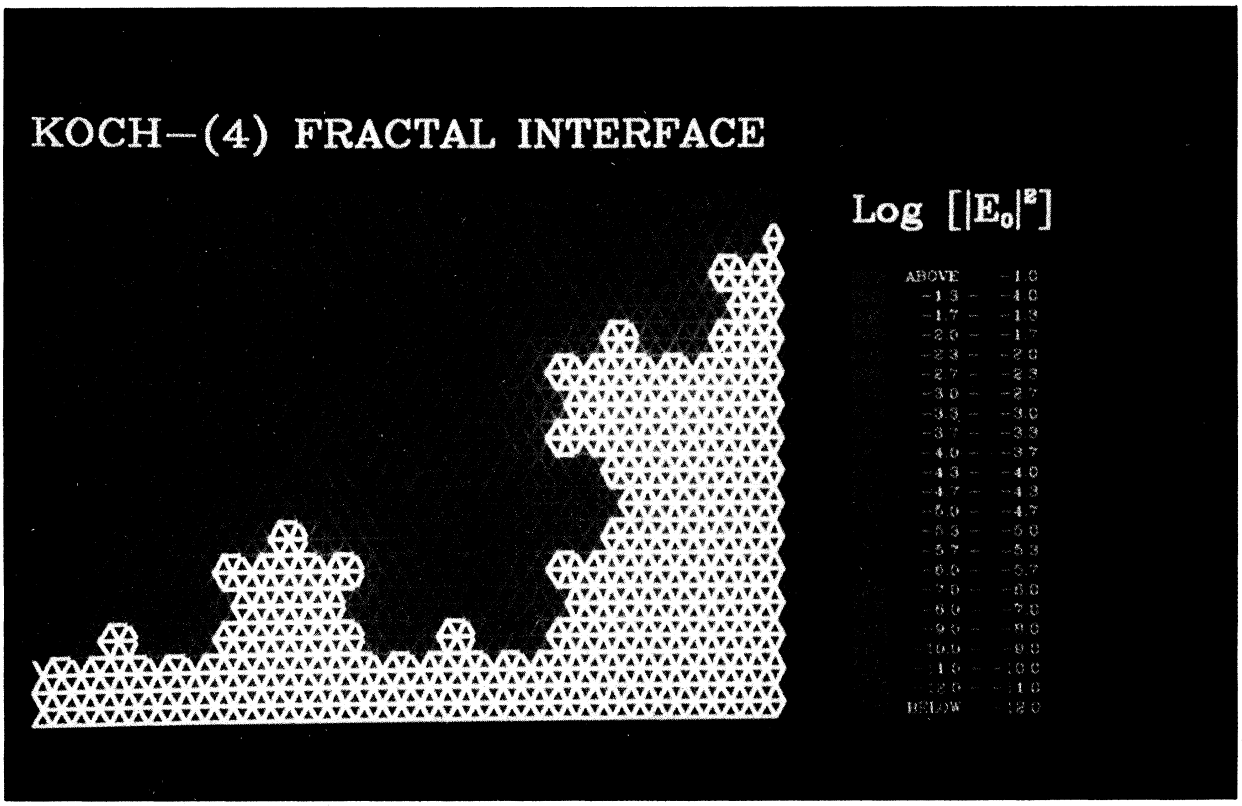

FIG. 8. Display of Joule losses for the fourth level of interfacial roughness. The grain is shown in white while the pore space is shaded from red to blue. Just one quarter of the two-dimensional model is shown.

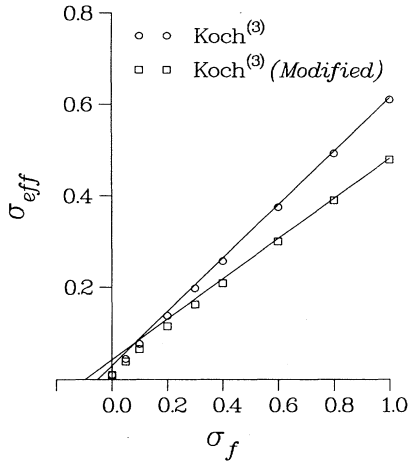

FIG. 9. Effective conductivities for the third-generation triadic–Koch-curve interface with and without the modification depicted in Fig. 6. The solid lines represent the high-salinity asymptotes.

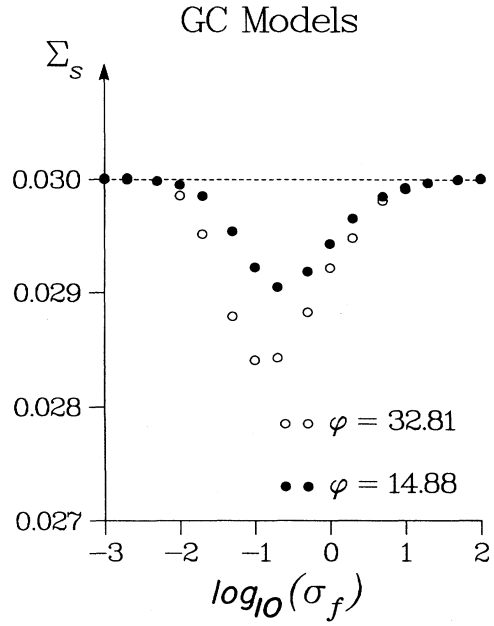

FIG. 10. The values of Σ_s deduced from the Padé approximant are compared with the exact result $\Sigma_s=0.03$ for the GC data originally presented in Fig. 2.

f, λ, F, and Λ have somehow been determined and we would like to know what, if any, salinity dependence the surface conductance has. In order to answer this last question, the curvature due strictly to geometrical effects must be adequately understood. We propose to deduce the salinity dependence, $\Sigma_s(\sigma_f)$, by fitting the Padé approximant, Eq. (10), to the measured data at each salinity and adjusting Σ_s until the two agree. To test the validity of the scheme, let us treat the numerical data of Figs. 2, 5, and 7 as if they were measured data. The "correct" answer, of course, would be $\Sigma_s \equiv$const for all values of σ_f. ($\Sigma_s=1$ for the two fractal models and $\Sigma_s=0.03$ for the GC model.) However, since the Padé approximant is not exact this will not be true except in the high- and low-salinity limits, where, by construction, we have

$$\lim_{\sigma_f\to\infty} \Sigma_s[\text{deduced}]=\Sigma_s[\text{exact}]+O(\sigma_f^{-1}) , \tag{14a}$$

and

$$\lim_{\sigma_f\to 0} \Sigma_s[\text{deduced}]=\Sigma_s[\text{exact}]+O(\sigma_f^{2}) . \tag{14b}$$

Thus the degree to which $\Sigma_s[\text{deduced}]\approx$const in the crossover region is a measure of how well the Padé approximant is working for the particular geometry.

The results corresponding to the GC data shown in Fig. 2 are shown in Fig. 10. In Figs. 11 and 12 analogous results are shown for the self-affine fractal and triadic–Koch-curve models. Several points emerge from these results: (a) As advertised in Eqs. (14), the deduced values of the surface conductance are correctly given in the high- and low-salinity limits where the Padé approximant is exact. (b) In the geometries where the surface roughness is relatively minor (i.e., the GC model, the averaged self-affine fractal, and the Koch(1) model) the Padé approximant reproduces the correct result, $\Sigma_s\approx$const, to high accuracy. (c) As the roughness is systematically increased, the accuracy of the Padé approximant decreases substantially. For the roughest of the self-affine geometries considered, the Padé approximant is essentially useless for the purpose of deducing the salinity dependence of Σ_s. Not only does the magnitude of the discrepancy increase, but the range in σ_f, over which that discrepancy is appreciable, broadens to lower values

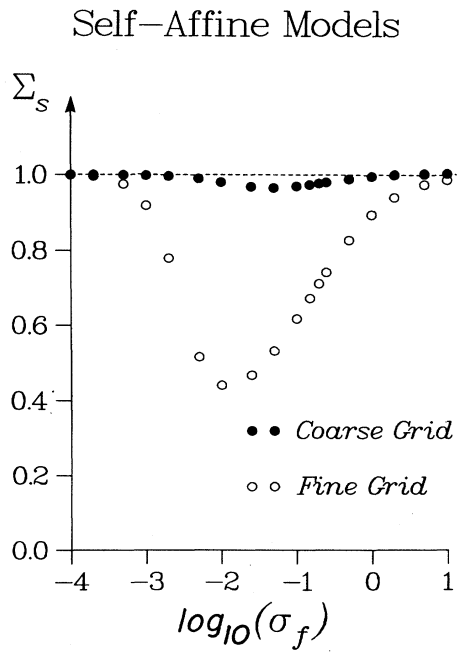

FIG. 11. The values of Σ_s deduced from the Padé approximant are compared with the exact result $\Sigma_s=1.0$ for the self-affine fractal data originally presented in Fig. 5.

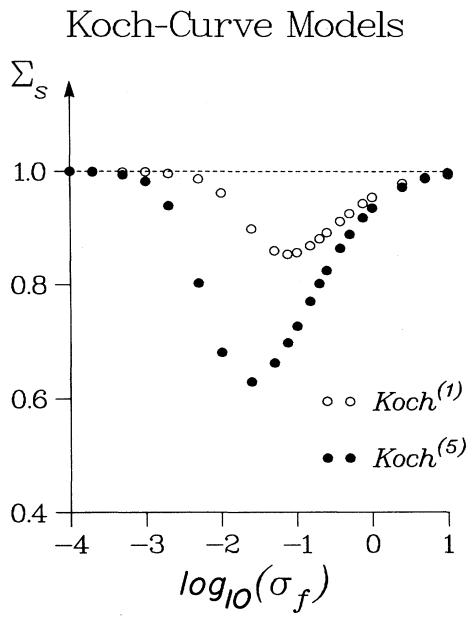

FIG. 12. The values of Σ_s deduced from the Padé approximant are compared with the exact result $\Sigma_s = 1.0$ for the triadic–Koch-curve data originally presented in Fig. 7.

of σ_f. In the GC models the maximum discrepancy occurs when $R \approx 1.0$; at these porosities the surface layer is almost discontinuous and the σ_{eff} versus σ_f passes nearly through the origin and approaches the straight line (5a) at high salinities. As R increases, $\sigma_{\text{eff}}(\sigma_f = 0)$ increases from 0, the entire $\sigma_{\text{eff}}(\sigma_f)$ curve has a more gentle character and the accuracy of the Padé approximant increases as can be seen in Fig. 10. Therefore, we conclude that, although the Padé approximant does an excellent job of reproducing the effective conductivity σ_{eff} considered as a function of σ_f, its use in the inverse problem, deducing the salinity dependence of Σ_s, is limited to pore geometries for which the surface roughness is not too severe; in these cases the Padé approximant does an excellent job and may be confidently applied in the analysis of experimental data.

IV. CONCLUSIONS

To summarize, we have presented the results of calculations based on three different models of electrolytic conduction in porous media. We have shown explicitly that (1) The constant A appearing in the empirical high-salinity formula can be highly dependent on the microgeometry of the pore space for rough surfaces. (2) The rougher the surface, the more apparent is the departure from linearity of σ_{eff} versus σ_f even if Σ_s is held constant; the accepted lore has it that curvature is due to the salinity dependence of Σ_s. (3) For cases in which the geometrical parameters f, λ, F, and Λ are known, a Padé approximant does an excellent job of interpolating into the region of curvature. The significance of this last result is that when these parameters are known from measurements (as described in Refs. 10 and 11) it is possible to deduce, for the first time, the salinity dependence of Σ_s.

ACKNOWLEDGMENTS

We have enjoyed several conversations with J. R. Banavar and P.-z. Wong during the course of this work. We are grateful to A. Zachary of Cray Research, Inc. (Mendota Heights, MN) for advice regarding our numerical calculations.

[1]A. G. Van der Put and B. H. Bijsterbosch, J. Colloid Interface Sci. **75**, 512 (1980).

[2]P. N. Sen, J. Chem. Phys. **87**, 4100 (1987).

[3]D. L. Johnson and P. N. Sen, Phys. Rev. B **37**, 3502 (1988).

[4]D. A. Weitz and M. Oliveria, Phys. Rev. Lett. **52**, 1433 (1984).

[5]C. E. Krohn and A. H. Thompson, Phys. Rev. B **33**, 6366 (1986).

[6]P.-z. Wong, J. Howard, and J.-S. Lin, Phys. Rev. Lett. **57**, 637 (1986).

[7]M. H. Waxman and L. J. M. Smits, SPE J. **8**, 107 (1968); C. Clavier, G. Coates, and J. Dumanoir, *ibid.* **24**, 153 (1984).

[8]J. A. De Waal, Proceedings of the 62nd Annual Technical Conference and Exhibition of the Society of Petroleum Engineers, Dallas, 1987 (unpublished) [see Fig. 3(a)]; H. H. Yuan and K. M. Diederix, Proceedings of the SPWLA Twenty-Eighth Annual Logging Symposium, July 1987 (unpublished).

[9]M. A. Mian and D. W. Hilchie, Log Anal. **23**, 10 (1982). These authors point out that the value of Q_v determined by chemical titration may depend on how finely the rock has been ground (i.e., on how much internal surface area has been exposed). Ideally, Q_v should include only those clay particles that are exposed to the pore fluid.

[10]D. L. Johnson, J. Koplik, and L. M. Schwartz, Phys. Rev. Lett. **57**, 2564 (1986).

[11]D. L. Johnson, T. J. Plona, and H. Kojima, in *Physics and Chemistry of Porous Media II (Ridgefield, 1986),* Proceedings of the Second International Symposium on the Physics and Chemistry of Porous Media, AIP Conf. Proc. No. 154, edited by J. R. Banavar, J. Koplik, and K. W. Winkler (AIP, New York, 1986). It is shown here how the geometrical parameters employed in this paper can be measured using superfluid ^{4}He acoustics. Depending on the pore size, F and Λ can be deduced from the measured speeds and attenuations of first and second sound or from the healing length in fourth-sound measurements. f and λ are related to the behavior of third-sound measurements in porous media.

[12]C. M. Bender and S. A. Orszag, *Advanced Mathematical Methods for Scientists and Engineers* (McGraw-Hill, New York, 1978).

[13]P. N. Sen, P. A. Goode, and A. Sibbit, J. Appl. Phys. **63**, 4832 (1988).

[14]M. R. J. Wyllie and P. F. Southwick, Trans. Metall. Soc. AIME **201**, 43 (1954); see also P. F. Worthington, Log Anal. **26**, 23 (1985).

[15]J. N. Roberts and L. M. Schwartz, Phys. Rev. B **31**, 5990 (1985).

[16]Po-zen Wong, in *Physics and Chemistry of Porous Media II (Ridgefield, 1986),* Proceedings of the Second International Symposium of the Physics and Chemistry of Porous Media, AIP Conf. Proc. No. 154, edited by J. R. Banavar, J. Koplik, and K. W. Winkler (AIP, New York, 1987), Sec. II.

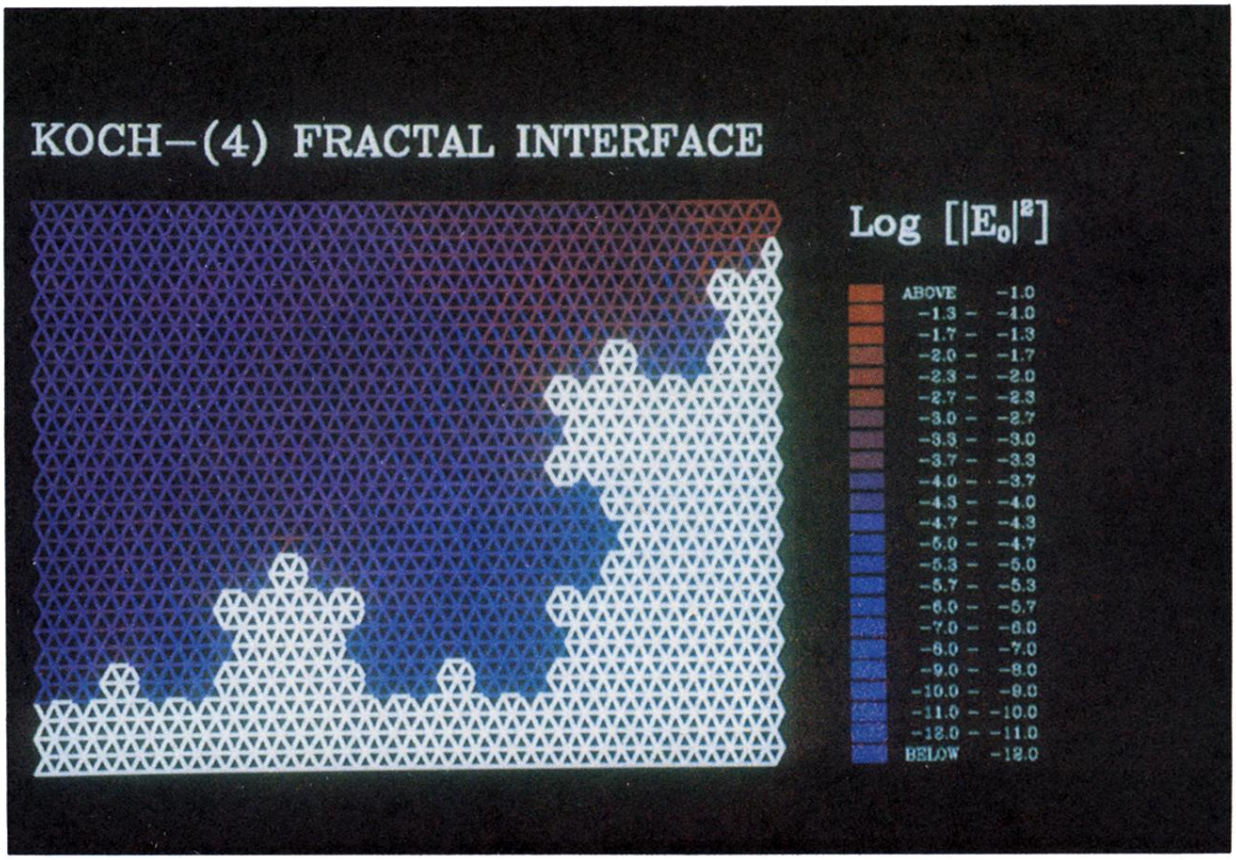

FIG. 8. Display of Joule losses for the fourth level of interfacial roughness. The grain is shown in white while the pore space is shaded from red to blue. Just one quarter of the two-dimensional model is shown.